

Spatial and Temporal Variability of the Three-Dimensional Flow around African Easterly Waves

ALAN BRAMMER AND CHRIS D. THORNCROFT

*Department of Atmospheric and Environmental Science, University at Albany,
State University of New York, Albany, New York*

(Manuscript received 1 December 2016, in final form 6 April 2017)

ABSTRACT

This study presents a large-scale trajectory analysis of African easterly waves (AEWs) across West Africa and the eastern Atlantic. Back trajectories were initialized at multiple pressure levels from in and around the vortex center of the AEW troughs to reveal the source regions of environmental inflow. The trajectory analysis highlights a changing influence of environmental air on AEW troughs. Over West Africa, monsoonal flow dominates with source regions of air from the southwest and east to northeast influencing the trough. As the AEW troughs leave West Africa, flow from the northwest becomes increasingly important. Cluster analysis highlighted that the contribution of trajectories from the northwest increased as the AEW troughs move westward and that this cluster also had high variability in environmental characteristics.

Correlation analysis of outgoing longwave radiation around the troughs with environmental characteristics 72 h earlier was conducted on 443 AEWs. This analysis reveals that the impact of the various source regions on convective activity within the AEW troughs is consistent with the cluster trajectory analysis. While the AEW troughs were over West Africa, convection was sensitive to midlevel equivalent potential temperature θ_e around the trough and to the northeast of the trough axis. Over the West African coast and Cape Verde basin, the correlation analysis captures the changing flow regime with sensitivity to θ_e west of the trough axis at midlevels and northwest at low levels. These results highlight that the cool and dry low-level northerly trade winds over the Canary and Cape Verde basin can be a crucial influence on AEWs as they leave West Africa.

1. Introduction

The structure and evolution of African easterly waves (AEWs) have been presented using many different approaches since the pioneering studies by Carlson (1969), Frank (1969), Burpee (1972, 1974), and Reed et al. (1977) among many others. These early papers, though using limited data, produced useful portrayals of the dynamic and thermodynamic structure of AEWs through composite analysis over multiple events. Since then global models and long-term reanalysis products have enabled further research to reveal more details through both composite and case study analysis of AEW structures and evolutions (e.g., Kiladis et al. 2006) as well as confirming the earlier results (e.g., Fink et al. 2004). This paper will present the structure of AEWs in a Lagrangian framework relying on back trajectories to analyze how AEW troughs interact with the environment as they traverse West Africa and the eastern Atlantic.

AEWs are the primary synoptic-scale disturbance over West Africa during the boreal summer months and their relationship with convection is well documented (e.g., Carlson 1969; Reed et al. 1977; Fink and Reiner 2003; Kiladis et al. 2006; Janiga and Thorncroft 2016). While the AEW troughs are over West Africa, the associated precipitation tends to occur in the northerly phase of the wave (west of the trough axis) south of the African easterly jet (AEJ; e.g., Duvel 1990; Diedhiou et al. 2001; Gu et al. 2004) and in the southerly phase of the wave north of the AEJ (northeast of the trough axis; e.g., Fink and Reiner 2003; Kiladis et al. 2006; Poan et al. 2013). Precipitation west of the trough axis is explained in part by the adiabatic forcing for ascent ahead of the trough (Thorncroft and Hoskins 1994) as well as the initiation of mesoscale convective systems and squall lines in or ahead of the trough that, propagating faster than the trough, propagate through the northerlies before dissipating (Janiga and Thorncroft 2016; Payne and McGarry 1977; Fink and Reiner 2003). As the low-level baroclinicity weakens west of the African coast, the precipitation maximum shifts toward the trough axis of

Corresponding author: Alan Brammer, abrammer@albany.edu

the AEWs (e.g., [Thompson et al. 1979](#)). Over the ocean, a primary modulator for convection around the AEW troughs has been shown to be the environmental relative humidity (e.g., [Bretherton et al. 2004](#)). [Janiga and Thorncroft \(2016\)](#) showed that not only was the column relative humidity important in modulating the precipitation in the AEW trough but it was also the main environmental variable influenced by the AEWs. The ability for the AEWs to modulate the moisture within the trough has also been proposed to be a fundamental process for providing sufficient environmental conditions for tropical cyclogenesis (e.g., [Dunkerton et al. 2009](#); [Wang et al. 2010](#)).

Over the Cape Verde basin and across West Africa there is a substantial meridional gradient of moisture with dry air from the Sahara and subsidence from mid-latitudes in close proximity to the AEW troughs and developing tropical cyclones. The influence of dry air entrainment into developing tropical cyclones or AEWs was suggested by [Dunion and Velden \(2004\)](#), who showed a relationship between dry air from the Sahara [Saharan air layer (SAL)] and tropical cyclone strength over the Atlantic. The SAL over the eastern Atlantic is characterized as a layer of warm, dry, and dusty air extending from the strong temperature inversion above the marine boundary layer up to around 500–400 hPa (e.g., [Prospero and Carlson 1972](#); [Carlson and Prospero 1972](#); [Karyampudi and Carlson 1988](#)). While the Sahara is a major source of dry and dusty air over the eastern Atlantic, [Braun \(2010\)](#) showed that dry air in the region is not always associated with SAL outbreaks and that subsidence in the region can have a large contributing factor to the relative humidity in the lower troposphere. There are also dust-free northerly trade winds at low levels along the West African coast undercutting the dusty SAL air above ([Carlson and Prospero 1972](#); [Brammer and Thorncroft 2015](#); [Schwendike et al. 2016](#)). The impact of dry (and dusty) air on tropical cyclones has been shown to vary across numerical simulation experiments and observational studies (e.g., [Braun et al. 2012](#); [Reale et al. 2014](#); [Rios-Berrios et al. 2016](#)). Both the origin (dustiness) and the vertical distribution of dry air are important for understanding the potential thermodynamic and microphysical impacts on convective systems. There has been substantial research investigating the possible impact of dry air on developing and developed tropical cyclones yet little in the context of AEWs over West Africa.

The strong meridional gradients of environmental moisture over West Africa and the Cape Verde basin combined with the changing structure of the AEWs creates a complex interaction between wave dynamics and environmental characteristics. The research presented in

this paper provides a kinematic view of how the propagating AEW troughs and the environment interact. The research utilizes trajectory analysis across a large number of waves to identify typical kinematic pathways for environmental air to reach the trough center. This analysis will highlight the regions that potentially have the largest impact on the convective and structural evolution of AEWs. This paper will present the large-scale trajectory pathways and source regions for AEWs over West Africa and the eastern Atlantic (i.e., the Sierra Leone, Cape Verde, and Canary Island basins) in an Eulerian framework ([section 3a](#)) followed by analysis in the Lagrangian framework ([section 3b](#)). Cluster analysis and the evolution of the trajectory pathways will be presented in [section 3c](#), with the impact of the environmental characteristics shown on a larger set of AEW troughs via a correlation analysis in [section 3d](#). The significance and impact of the results are discussed with main conclusions in [section 4](#).

2. Data and methodology

a. Data

This research uses the combined reanalysis datasets from the National Centers for Environmental Prediction (NCEP): the Climate Forecast System Reanalysis (CFSR; [Saha et al. 2010](#)) for 1979–2011 and ongoing operational CFS, version 2, for 2011–present ([Saha et al. 2014](#)). These data have a consistent temporal resolution of 6 h with a horizontal resolution of 0.5° and 33 levels in the vertical, with 25-hPa vertical spacing between 1000 and 750 hPa. The CFSR, like other reanalysis products, relies on the assimilation of observations and short-term forecasts from the previous initialization time. Because of the relatively sparse observation network over West Africa reanalysis products are less constrained by the observations and model biases are evident. [Janiga and Thorncroft \(2013\)](#) showed that the CFSR has a wet bias over the eastern Atlantic in precipitation and an associated overintensification of low-level vorticity from diabatic heating compared to the Tropical Rainfall Measuring Mission, version 3b42 ([Huffman et al. 2007](#)), precipitation and heating profiles as well as the European Centre for Medium-Range Weather Forecasts (ECMWF) interim reanalysis (ERA-I; [Dee et al. 2011](#)). [Roberts et al. \(2015\)](#) also showed that the CFSR has a systematic southward bias of the intertropical discontinuity (ITD) over the Sahel; however, the largest differences shown were likely due to disagreements in the location of the ITD rather than large-scale regional biases. The National Climatic Data Center daily interpolated outgoing longwave radiation

(OLR) was used as a metric for convective activity. This dataset also spans 1979–present with 1° horizontal resolution and combines multiple bias-corrected radiance estimates from available satellites over the data period (Lee 2011; Lee et al. 2014). Anomalies for both datasets are calculated from a smoothed 1979–2011 climatology utilizing the first four harmonics of the mean 6-hourly or daily fields.

b. Wave tracking

AEWs were defined and tracked following the methodology used in Brammer and Thorncroft (2015). This method involves initially tracking 2–10-day filtered curvature vorticity at 700 hPa using a Hovmöller diagram. These filtered tracks, which are a function of time and longitude, are then used to refine the tracked location to three dimensions using raw 700-hPa curvature vorticity (averaged over a 500-km radius). The somewhat large radius helps to smooth out small mesoscale systems and also filters out weak AEWs with very short wavelengths. The subset of AEWs used for the trajectory analysis in this paper will be further reduced to only include waves that were defined as “favorable” for tropical cyclogenesis over the eastern portion of the Atlantic main development region (east of 45°W). These 86 waves are identical to those featured in the composite analysis of Brammer and Thorncroft (2015), which are defined as having a combination of increased 850-hPa relative vorticity, upper-level divergence, ascent throughout the middle troposphere, and a positive upper-level temperature anomaly as they leave the West African coast during August or September. These waves are coherent in structure and were objectively tracked from 5° to 45°W ; therefore, they create a consistent dataset of waves for the analysis of the evolution of the large-scale flow across different locations.

c. Trajectories

Trajectories used in this paper were all calculated using the National Oceanic and Atmospheric Administration (NOAA)/Air Resources Laboratory (ARL) Hybrid Single-Particle Lagrangian Integrated Trajectory model (HYSPLIT; Draxler and Hess 1997, 1998; Stein et al. 2015) with the reanalysis fields from CFSR used as input. The trajectories are calculated using the full three-dimensional (3D) winds from the reanalysis. The largest source of error in 3D kinematic trajectories has been shown to be the interpolation of the vertical velocity field, though using the model vertical velocity is more accurate for absolute location errors and conservation of variables along the trajectory path compared to trajectories calculated along either isoeta or isentropic surfaces (Stohl et al. 1995; Stohl and Seibert 1998).

The CFSR fields used here have 33 vertical levels, exceeding the recommended minimum of 9 vertical levels for accurate trajectories when using 6-h temporal and 0.5° horizontal resolution suggested by Stohl et al. (1995). Consequently, the reanalysis fields should be able to adequately represent the synoptic-scale motion analyzed here. Recent papers have shown that CFSR and other reanalysis products provide sufficient input data to analyze synoptic-scale meteorological phenomena around tropical cyclones (e.g., Galarneau et al. 2010; Schenkel and Hart 2015) as well as moisture advection diagnosed by trajectories (e.g., Pierrehumbert and Roca 1998; Roca et al. 2005; Sjoström and Welker 2009; Ersek et al. 2010; Deshpande et al. 2015). Reanalysis products are, however, not dynamically consistent from one time to another and therefore substantial errors can arise from this dynamical inconsistency for the conservation of thermodynamic variables along the trajectories (Stohl and Seibert 1998). Given the consistent results provided by the trajectory calculations and the physical reasoning behind the results, the authors do not feel like this significantly impacts the main results in this research. Boundary layer processes and interpolation of the terrain also pose further errors. Therefore, in post-processing, any trajectories that came within 500 m of the terrain were removed from the analysis. These surface-interacting trajectories accounted for about 14% of all trajectories launched.

Trajectories were initialized around the center of the trough for each AEW at three locations across West Africa. These locations were determined relative to each trough’s passage at the coast (16°W). The times chosen were 36 h downstream (west) of the coast, over the coast (0 h), and 36 h upstream (east) of the coast. To avoid the confusion of having multiple time units, the locations will be referenced by the mean longitude of the troughs at each time hereafter (i.e., 25° , 16° , 6°W , respectively). At each location, trajectories were initialized across a $3^\circ \times 3^\circ$ horizontal grid at 0.5° spacing centered on the trough location and at 11 vertical levels, spanning from approximately 900 to 400 hPa at 50-hPa increments. This grid creates 539 trajectories per wave per location, resulting in a total of over 139 000 trajectories. Truncation errors and any errors due to initial location should therefore be minimized by the large number of trajectories analyzed (Merrill et al. 1985; Harris et al. 2005). The composite low-level structure of the waves at each location used in this analysis along with the box within which trajectories were initialized is shown in Fig. 1.

Trajectories were integrated backward for a total of 120 h. To clarify terminology, trajectories will be referred to in the chronological sense and therefore

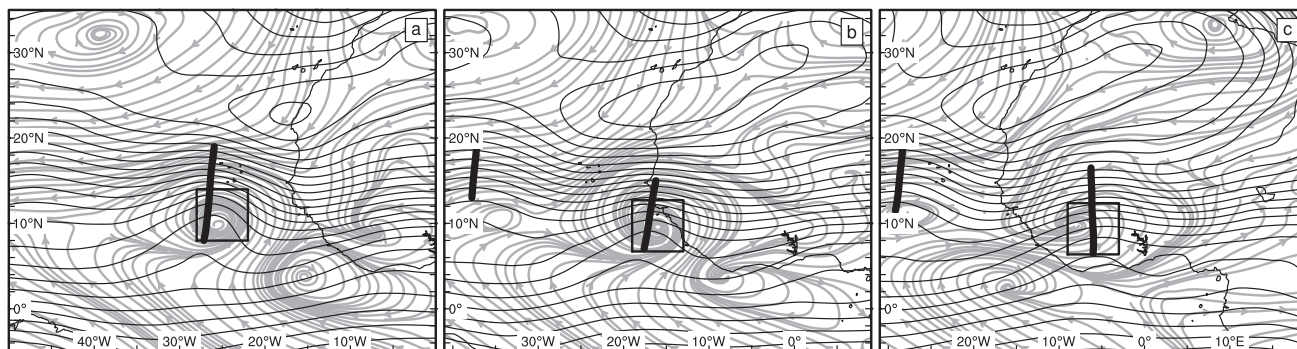


FIG. 1. Composite AEWs at three locations. Black contours show 700-hPa streamfunction, thick black contour shows objective trough line (Berry et al. 2007), and gray streamlines show 850-hPa wave-relative wind. Composite of 86 AEWs are shown as the troughs cross three locations: (a) 25°W, (b) 16°W, and (c) 6°W.

source/origin will refer to the trajectory locations 120 h before reaching the trough. Ingestion or initialization location will refer to the locations within the trough, where the back trajectories were initialized.

In postprocessing, the trajectories were then also adjusted to a wave-relative reference frame. This adjustment involved subtracting the location of each AEW trough interpolated to 1-h intervals. If the track of the wave did not extend for the full 120 h, the mean phase speed of the wave was used to extrapolate the track backward in time.

For the Eulerian compositing analysis, each trough was relocated to the mean location of all troughs at that time. The trajectories were also subject to this small uniform shift over their entire integration. Geographical references are with respect to the mean trough location at that compositing time. This trough-relative adjustment is relatively minor though ($\leq 2.5^\circ$) so the general geographical references are still applicable.

Trajectory compositing was performed to visualize the mean flow vector of the trajectories relative to a fixed grid. This compositing method involved calculating the two-dimensional flow vector of the trajectories at each time and then compositing the horizontal components to a 0.5° grid. The streamlines are then computed on the resulting mean flow. The streamlines therefore represent the mean flow of trajectories at a given location and time, presenting a unique representation of the flow approaching the AEW; the only data points included are from trajectories that will reach the center of the trough.

d. Cluster analysis

Cluster analysis has been used across numerous studies to quantify and analyze the large-scale flow regimes from trajectory analysis in gridded atmospheric datasets (e.g., Moody and Galloway 1988; Harris and

Kahl 1990; Dorling et al. 1992; Cape et al. 2000; Kassomenos et al. 2010). The type of clustering algorithm and the variables used to cluster can influence the resulting clusters; therefore, while it is an objective technique, there are subjective options in how it is applied. For this study, a *K*-means algorithm was used and the trajectories were clustered on their origin characteristics using the wave relative latitude, longitude, and equivalent potential temperature θ_e for a pseudovertical coordinate. The *K*-means algorithm groups data into a defined number of clusters by minimizing the within-cluster sum of squares (distance to the cluster mean) and thus maximizing the distance between clusters as well (e.g., MacQueen 1967; Witten and Tibshirani 2010). Because of a lack of objective methodology for choosing the optimum number of clusters, analysis was conducted on between four and eight clusters. These tests revealed that five clusters were optimal for representing the main pathways and source regions. While increased clusters provide more detail, the overlap in interpreting the results also increases.

3. Results

a. Eulerian trajectory composite analysis

The density of the 120-h backward trajectories for the three trough locations are shown in Fig. 2. This figure shows the geographical extent of the air being ingested by the AEW troughs over 5 days, as well as the predominant large-scale inflow routes toward the AEW troughs. The boxes in each plot display the region over which trajectories were initialized within AEW troughs at hour 0. The dashed line in each plot represents the mean or extrapolated location of the troughs 120 h earlier.

When the AEW troughs are around 6°W, the backward trajectories show that air within the trough has

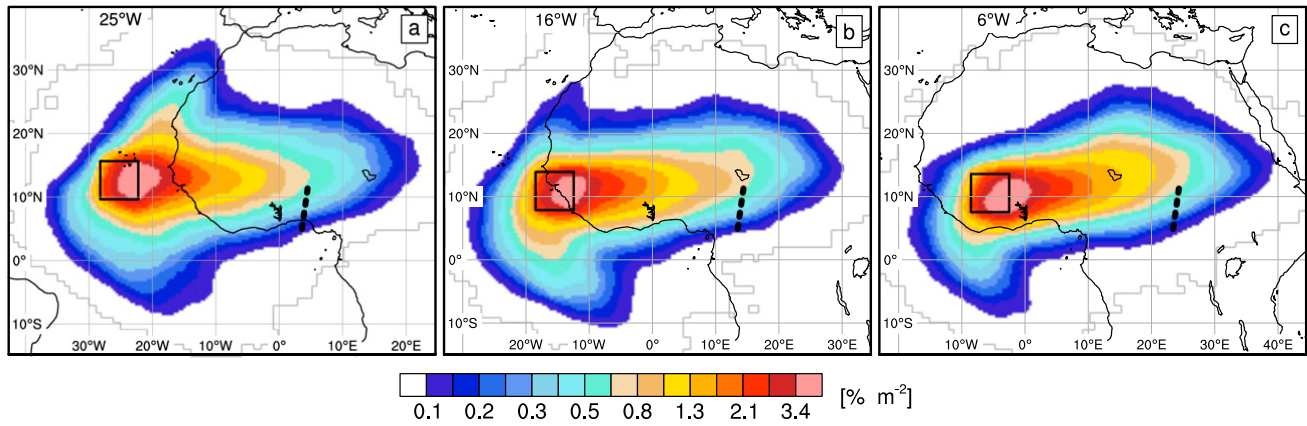


FIG. 2. Density of trajectories composited over 120-h backward integration from trough centers. Trajectories are shown with respect to three initialization locations: (a) 25°W, (b) 16°W, and (c) 6°W. Box encompasses 3° × 3° initialization grid around the troughs. Dashed thick line represents mean location of the AEW troughs 120 h before trajectories were launched. Densities have been normalized by the area of the underlying 0.5° grid.

been sourced along two main pathways (Fig. 2c). The primary pathway at this location, extends to the east of the AEW trough and is then split between ascent and southerly flow from over the eastern Sahara and subsiding easterly flow along the AEJ at 700–600 hPa coincident the AEW troughs (Fig. 3c). The secondary route at this location is air from the south, over the Gulf of Guinea, associated with the monsoonal southerlies. Trajectories along this route are on average between 900 and 800 hPa over the ocean, approaching the troughs from the west at low levels (Fig. 3c).

As the AEW troughs leave the West African coast (Figs. 2a,b), a third pathway for trajectories approaching the troughs is evident. Trajectories from the north propagate south along the northwest African coastline at low levels with mean pressure between 900 and 800 hPa (Figs. 3a,b). This low-level flow is sourced from north of 30°N associated with the

trade winds on the eastern edge of the Atlantic subtropical ridge. Low-level flow along this route is typically dust free with non-Saharan origins, though when the flow crosses overland it is able to pick up small but significant quantities of dust (Carlson and Prospero 1972). Also, over the eastern Atlantic, on the western periphery of the streamlines (20°N, 20°W; Fig. 3a), there is a slight indication of in situ subtropical subsidence after which the trajectories indicate northerly flow into the AEW troughs. This subtropical subsidence was argued by Braun (2010) to be an important source of dry dust-free tropical air not associated with SAL outbreaks.

This composite analysis of the back trajectories has highlighted the changing kinematics associated with the large-scale sources of air that enter the AEW troughs as they propagate over West Africa and the eastern Atlantic. Over West Africa the primary sources

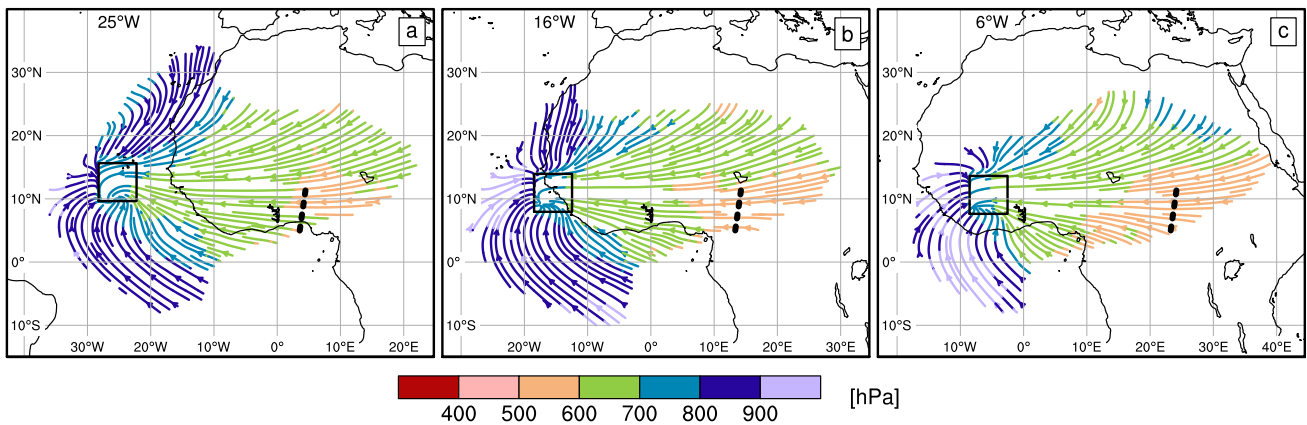


FIG. 3. Mean pressure (colored) and vector flow (streamlines) of trajectories along 120-h backward integration from AEW trough center per 1° grid. Trajectories are shown with respect to three initialization locations: (a) 25°W, (b) 16°W, and (c) 6°W. Annotations for plots as in Fig. 2.

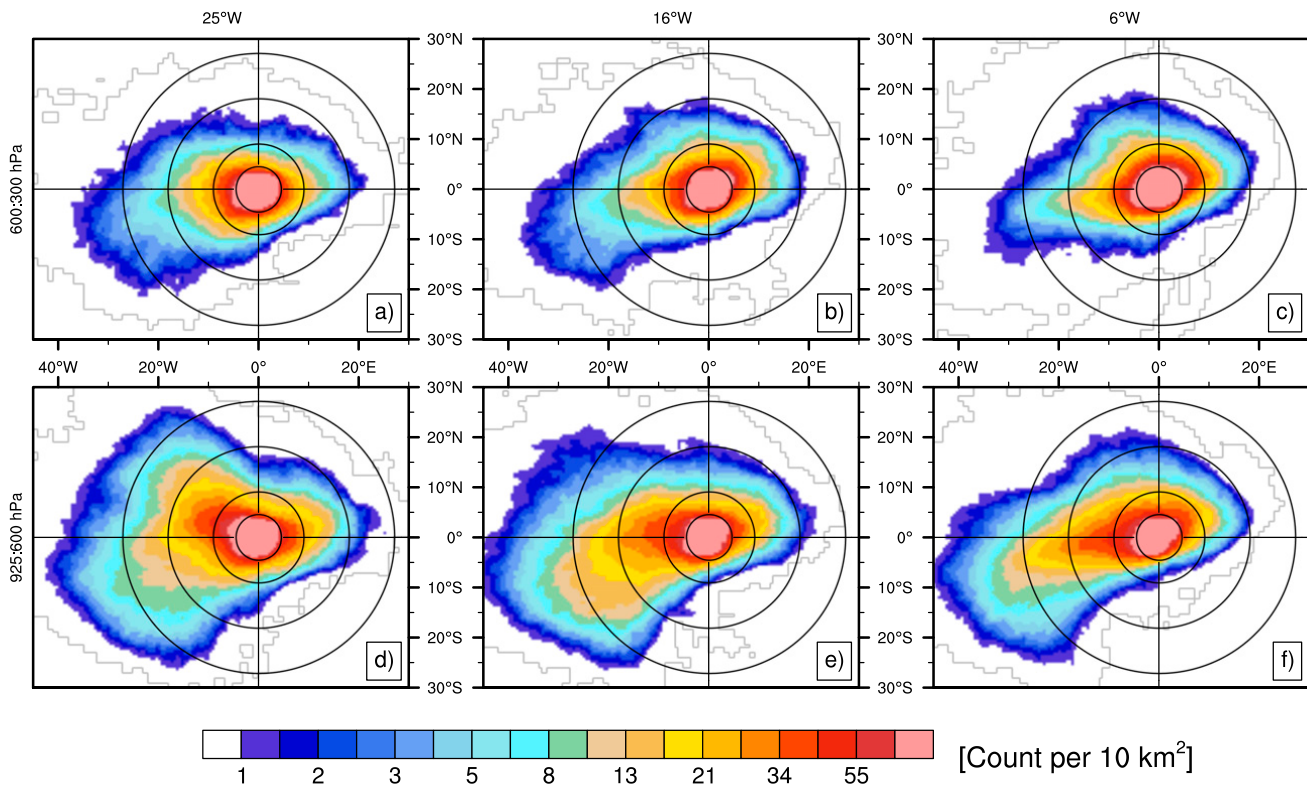


FIG. 4. Density of trajectories over a backward integration of 120 h in wave-relative frame. Trajectories have been shifted to be trough relative throughout the integration. Columns contain plots with respect to three initialization locations: (a) 25°W, (b) 16°W, and (c) 6°W. Rows contain plots with respect to the initialization level of trajectories [(a)–(c) 600–300 hPa and (d)–(f) 925–600 hPa]. Range rings are shown at 500, 1000, 2000, and 3000 km from center. Densities have been normalized by the area of the underlying 0.5° grid.

of air for the AEW troughs are from the south and east, while over the eastern Atlantic northerly flow becomes an increasingly dominant source of flow reaching the troughs' centers.

b. Lagrangian trajectory composite analysis

To visualize the inflow toward the AEW troughs, the trajectories have been shifted with respect to the framework of the moving troughs at each hour during the backward integration (Fig. 4). This shift therefore highlights the air masses, relative to the location of each trough, which will be ingested by the troughs over the following 120 h. Trajectories initialized between 600 and 300 hPa are shown in Figs. 4a–c. These plots show that the ingested air generally remains within about 2000 km of the trough center over the 120-h integration. The main trajectory routes toward the trough center are also relatively consistent across the three locations shown. The midlevel trajectories within the trough are consistently sourced from the southwest and northeast.

Trajectories initialized in the lower levels (925–600 hPa) of the AEW troughs show more regional

variability (Figs. 4d–f). Over the eastern Atlantic and West African coast, the flow from the northwest and southwest quadrants reaches out to 3000 km away over the 120-h integration (Figs. 4d,e). However, in the eastern quadrants, other than the trajectories from due east, there is very little flow from the southeast beyond 1000 km or the northeast beyond 2000 km. When the troughs are over West Africa, flow from the northwest beyond 1000 km is also very limited, with the main route into the low levels being primarily from southwest of the trough (Fig. 4f).

The previous figures have shown the spatial routes for environmental inflow toward the AEW troughs; however, by compositing over the whole 120-h integration, the temporal aspect of the inflow has been masked. Figure 5 shows the median time in hours from the trough center along the trajectories, or this can be interpreted as the number of hours it will take for air at a specific location to reach the AEW trough. Back trajectories initialized between 600 and 300 hPa show a relatively consistent radial gradient for the time it takes trajectories to reach the trough center. Trajectories

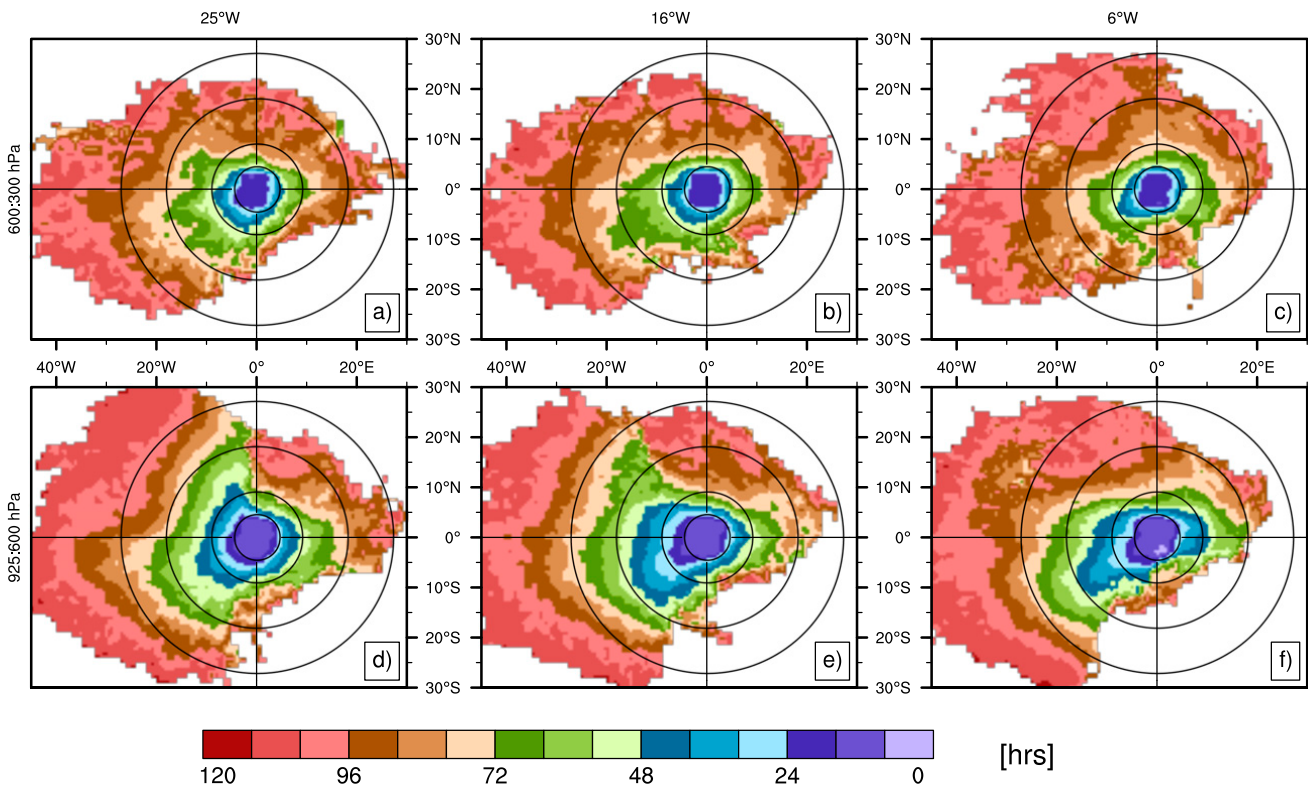


FIG. 5. Median number of hours from trough center for all waves and levels. Columns contain plots with respect to three initialization locations: (a) 25°W, (b) 16°W, and (c) 6°W. Rows contain plots with respect to the initialization level of trajectories [(a)–(c) 600–300 hPa and (d)–(f) 925–600 hPa]. Range rings are shown at 500, 1000, 2000, and 3000 km from the center.

from any direction within the inner 1000 km are likely to reach the center of the trough within 72 h. As the troughs cross the West African coast, trajectories from the west and southwest have a slightly faster approach covering up to 1500 km within 72 h (Fig. 5a).

At the lower levels, trajectories from the west and southwest have a faster approach to the center with trajectories covering up to 2000 km within 72 h (Figs. 5d–f). This result is due to the combined westward propagation of the AEW troughs and the background westerly flow. Over the eastern Atlantic, the flow from the north is advected equatorward into the path of the AEW troughs on a relatively fast route to the center, with the trajectories at 2000 km north of the trough also reaching the center within 72 h (Figs. 5d,e). The distances in these plots represent the Euclidean distance between the trajectories at a specific time and their initialization location. The total distance traveled by a trajectory is typically around 50% greater than the respective Euclidean distance at that time.

These figures have shown that over West Africa, AEW troughs mainly comprise air sourced from over East Africa that propagates along the easterly jet with

the troughs and from low-level monsoonal inflow from the Gulf of Guinea. This flow is a typical climatological view of the West African monsoon, although the trajectories have not shown a substantial source of trajectories from north of the AEW troughs while they are over the continent. As the troughs move over the coast and the eastern Atlantic, low-level flow from the northwest becomes increasingly dominant with a relatively fast route for air to reach the troughs' centers. This inflow pathway was predominantly between 800 hPa and the surface, over the ocean and close to the coastline. This low-level non-Saharan air is likely dust free and undercutting the typical dusty air from the Sahara (Carlson and Prospero 1972). A detrimental impact of this low-level air was recently suggested by Brammer and Thorncroft (2015) and Schwendike et al. (2016) for eastern Atlantic tropical cyclogenesis from AEWs. Although this route for trajectories is low in the atmosphere, the low-level trade wind flow remains above the boundary layer and thus separated from the oceanic surface fluxes due to the very shallow marine boundary layer; over the Mauritanian upwelling region the boundary layer can be as shallow as 200–300 m (Lee et al. 2010).

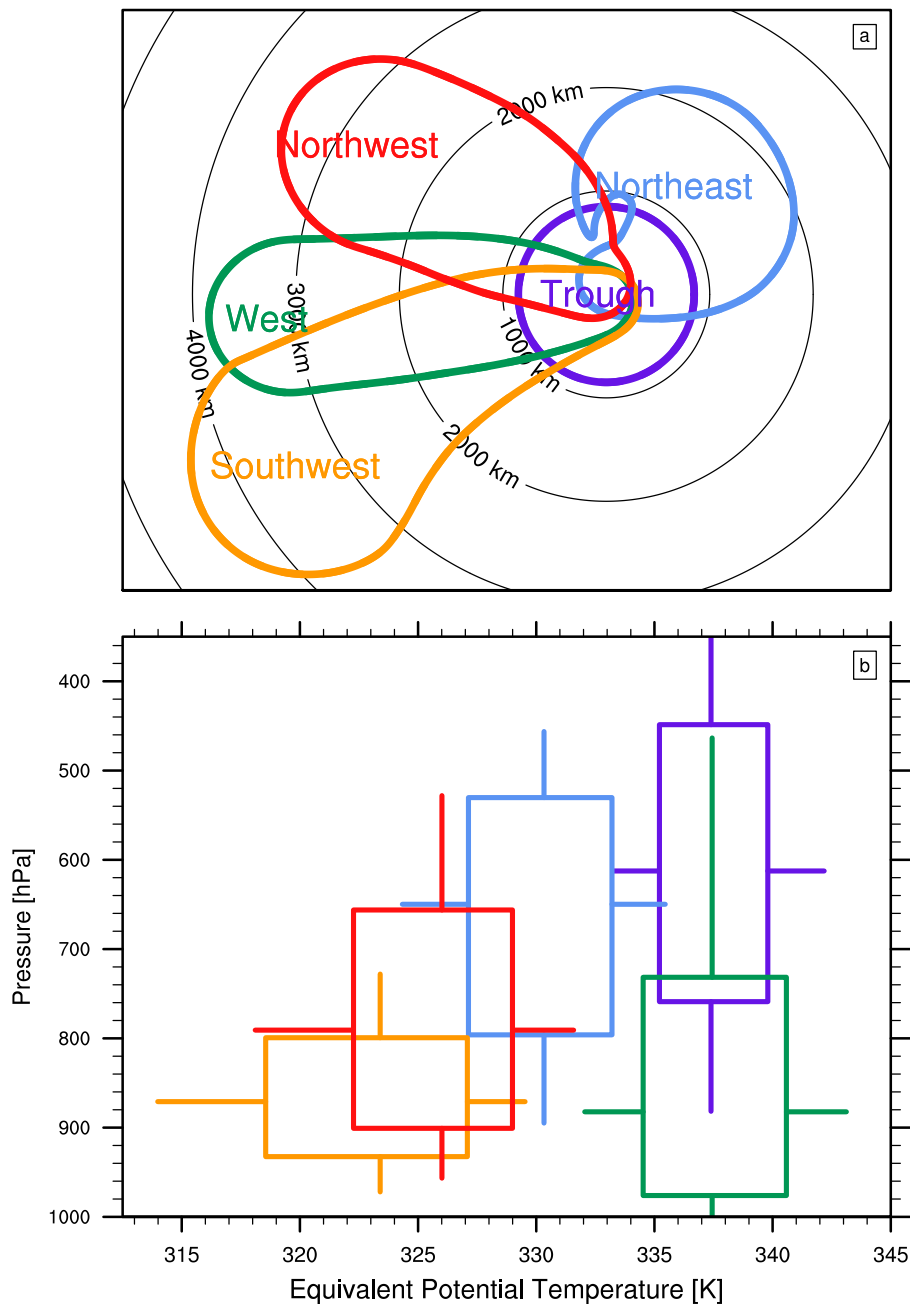


FIG. 6. (a) Geographical distribution of clustered trajectory source regions in trough-relative frame. Cones represent the origin and flow route of each cluster of the 120-h back trajectory. Cones are calculated as the median trajectory ± 1 standard deviation of across route variability. (b) Two-dimensional box-and-whisker plots of pressure and equivalent potential temperature for trajectory source characteristics within each cluster. Boxes contain the inner quartile range and whiskers extend to the 5th and 95th percentile.

c. Cluster analysis of trajectories

The composite analysis of trajectories highlights different routes toward the troughs at different levels and how this varies across different regions. To quantify changes in the characteristics and contribution of the relative source regions, the trajectories were clustered

into five clusters with respect to the -120 -h trough relative location and equivalent potential temperature θ_e using a K -means algorithm. Figure 6 shows the trough relative source regions and flow routes for each cluster of trajectories. As three variables were used to cluster the trajectories there is some overlap of the clusters in both the spatial map (Fig. 6a) and the thermodynamic

plot (Fig. 6b); however, points that overlap spatially should be distinct thermodynamically and vice versa.

The five cluster source regions can be briefly summarized as follows:

- Trough: Trajectories originate around the level of the AEJ between 750 and 450 hPa, with relatively high θ_e and remain within the trough circulation.
- Northeast: Trajectories originate around 1000–2000 km away from the trough center between 800 and 500 hPa. These trajectories have lower θ_e than the trough trajectories, consistent with reduced moisture content farther north.
- West: Low-level trajectories between the surface and 750 hPa, with high θ_e . These trajectories are mostly sourced from over the Sahel and tropical eastern Atlantic.
- Southwest: Trajectories originating between 950 and 800 hPa, over the Gulf of Guinea, and equatorial Atlantic. Low θ_e due to the relatively cold sea surface temperatures of the Gulf of Guinea cold tongue.
- Northwest: Trajectories entrained from 1000 to 4000 km away from the trough center. Lower θ_e (due to low humidity) than the trajectories in the trough and from the west, originating between 900 and 700 hPa over the eastern Atlantic and western edge of the Sahara.

Figure 7 quantifies the distribution of relative humidity for trajectories from each source region and the contribution of trajectories from each cluster with respect to the total number of trajectories reaching the AEW troughs. Trajectories associated with the trough cluster have consistently high relative humidity across the three locations, though the percentage of trajectories that are classified in the trough cluster decreases as the waves move westward (from a median contribution of 33%–24%). The relative humidity of trajectories from the northeast is also consistent across West Africa (around 40%), with a minor decrease of around 5% in the total contribution from this cluster as the waves move westward. The west and southwest clusters both have high relative humidity values at the source regions with no obvious trends in the contribution or humidity from each of the clusters as the AEW troughs move westward. Trajectories from the northwest have low relative humidity over West Africa, between 25% and 40%, with a clear trend toward higher humidity as the waves move westward, though still limited to below around 45% as the troughs reach 25°W. The contribution of trajectories from the northwest, however, shows a substantial increase as the AEW troughs move westward. Over West Africa, the northwest cluster only contributes around 10% of the total trajectories; once

over the eastern Atlantic this contribution has increased to around 15% and in some cases up to 30% of the total trajectories.

Figure 8 shows the time series for the cluster median and interquartile range (IQR) for pressure (Figs. 8a,b), θ_e (Figs. 8c,d), and θ (Figs. 8e,f). Trajectories clustered in the trough region show gradual ascent from -120 to 0 h with the cluster median pressure decreasing from 625 to 525 hPa (Fig. 8a). The distribution of the trajectories within the cluster also decreases during this time indicating that trajectories are converging to the midlevels of the trough (Fig. 8b). The evolution of θ_e for the trough cluster shows very little change over the 120 h, with a consistent 337-K median and IQR between 4 and 5 K (Figs. 8c,d). Potential temperature, however, does show an increase of 7 K indicating diabatic processes occurring with the trough of the wave.

Trajectories from the northeast show a similar evolution in pressure to the trough cluster, with the median ascending approximately 75 hPa over the 120 h (Fig. 8b). Converse to the trough trajectories, however, these northeast trajectories originate with lower θ_e (located geographically over the eastern Sahara) and experience a slight increase in moisture over time with θ staying approximately isentropic over the integration. The θ_e increase exhibited in this cluster largely occurs during hours -120 to -72 of the trajectory calculation. During this time the IQR of the trajectory pressure falls rapidly from over 250 to 150 hPa while the median stays steady. This suggests that there is likely a number of trajectories being lifted along the isentropes toward the median pressure of the cluster. This gradual increase in the cluster median θ_e could also be due to subgrid-scale mixing, for which the reanalysis and trajectory calculations are unable to account.

Trajectories from the west, southwest, and northwest are mostly from lower levels than the clusters for the trough and northeast, with all three clusters exhibiting an increase in altitude of 100–200 hPa as the trajectories approach the trough between hours -48 and 0 (Fig. 8a). For the trajectories from the west and southwest, this ascent is coincident with an increase in θ suggesting that convection and diabatic heating are associated with trajectories in this cluster over the last 24 h prior to reaching the trough center. The southwest cluster was shown to exhibit the lowest θ_e at hour -120 in Fig. 6b. The evolution here shows that while the trajectories in this cluster are very low in the atmosphere between the surface and 900 hPa and maintaining a consistent θ they are accumulating moisture. During this evolution the median θ_e increases from 323 to 337 K, close to the climatological value for boundary layer θ_e over the equatorial Atlantic and Sahel. However, although the cluster

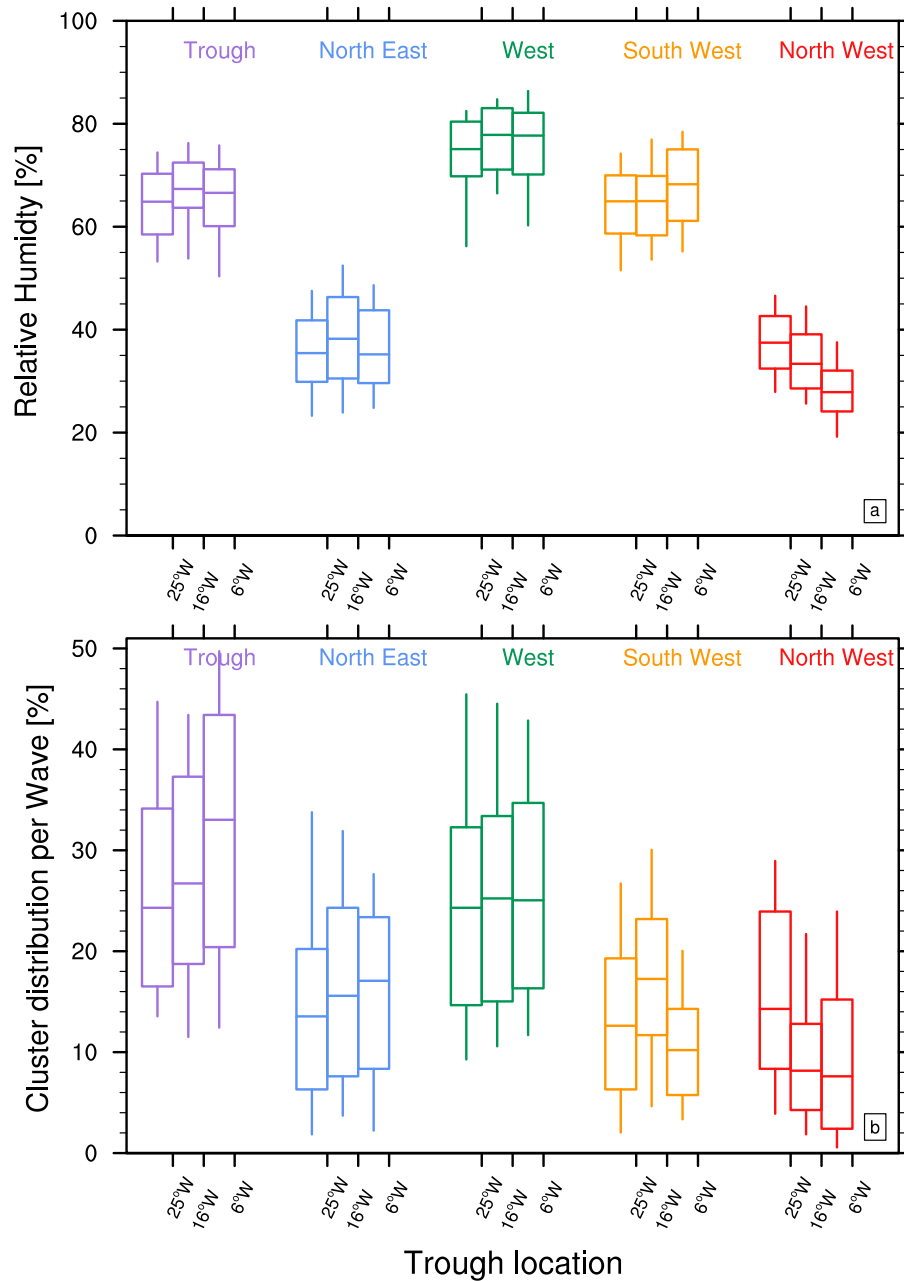


FIG. 7. (a) Distribution of trajectory relative humidity at -120 h per cluster and per initialization location. (b) Distribution of the contribution of trajectories from each cluster per wave. Percentages are calculated relative to the trajectories for each individual wave. Boxplots show interquartile range, median, and 5th and 95th percentiles.

median exhibits an increase in θ_e , the northwest cluster still has the lowest median θ_e of 331 K at -48 h. In the last 48 h as the trajectories approach the trough, this cluster also has the largest θ_e IQR of 5–8 K (Figs. 6c,d). Although the oceanic boundary layer is relatively shallow north of Dakar along the African coast, as the trajectories approach the trough they will be over warmer SSTs as well as the warm and moist Sahel. The cluster median pressure of 800–700 hPa, with an IQR of over

200 hPa, suggests that trajectories in this cluster begin to interact with the boundary and their characteristics begin to be modified as they approach the trough center (Figs. 6a,b).

The previous section has shown the primary pathways for trajectories reaching the AEW troughs over West Africa and the evolution of their properties. The cluster analysis simplified the routes of inflow to five distinct regions with different spatial and

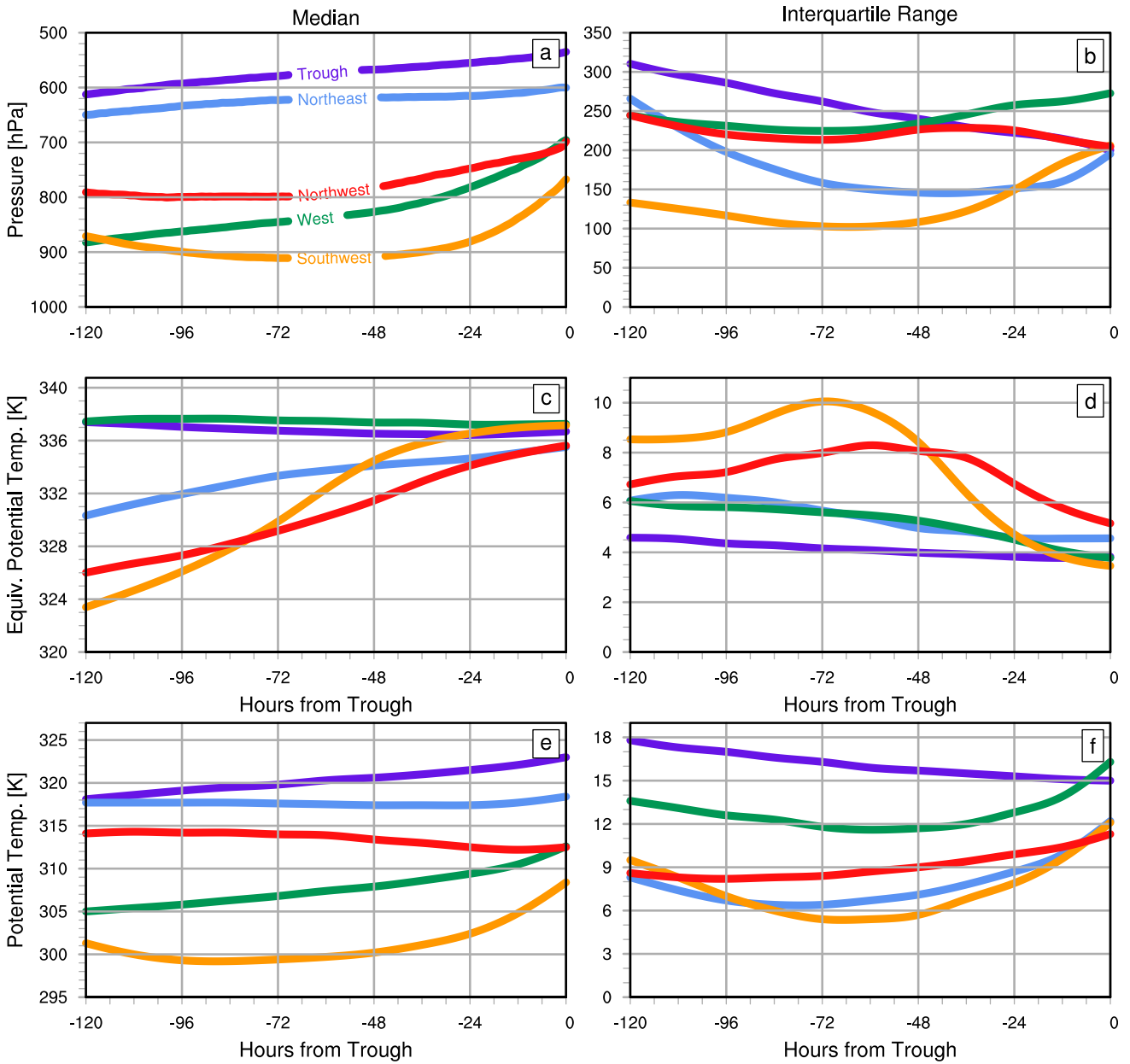


FIG. 8. Evolution of trajectory characteristics per cluster as the trajectories approach the trough center. (left) Median cluster characteristic and (right) the interquartile range for each cluster. The evolution of (a),(b) pressure level; (c),(d) θ_e ; and (e),(f) θ is shown for the each cluster. Line colors are indicated in (a).

thermodynamic origins. This analysis provides a direct causal link between how the environment around the AEW troughs could impact the characteristics and evolution of the trough and its associated weather. The cluster analysis has highlighted the potential role of moisture flux from the west and southwest contributing to precipitation around the trough. The contribution of dry air from the northeast at midlevels decreases as the waves move westward while the low-level contribution of dry air from the northwest increases.

It is expected that while the moisture flux or the flux of θ_e from the west and southwest clusters are important for convective activity, the northwest cluster has the largest variability and also lowest θ_e at low levels when reaching the trough; therefore, variability in this area may have the largest impact on trough-scale characteristics. The influence of this environmental air was shown over the Atlantic for developing cyclones from AEWs by [Brammer and Thorncroft \(2015\)](#). To assess this hypothesis, a larger-scale analysis will use the source regions and trajectory routes and

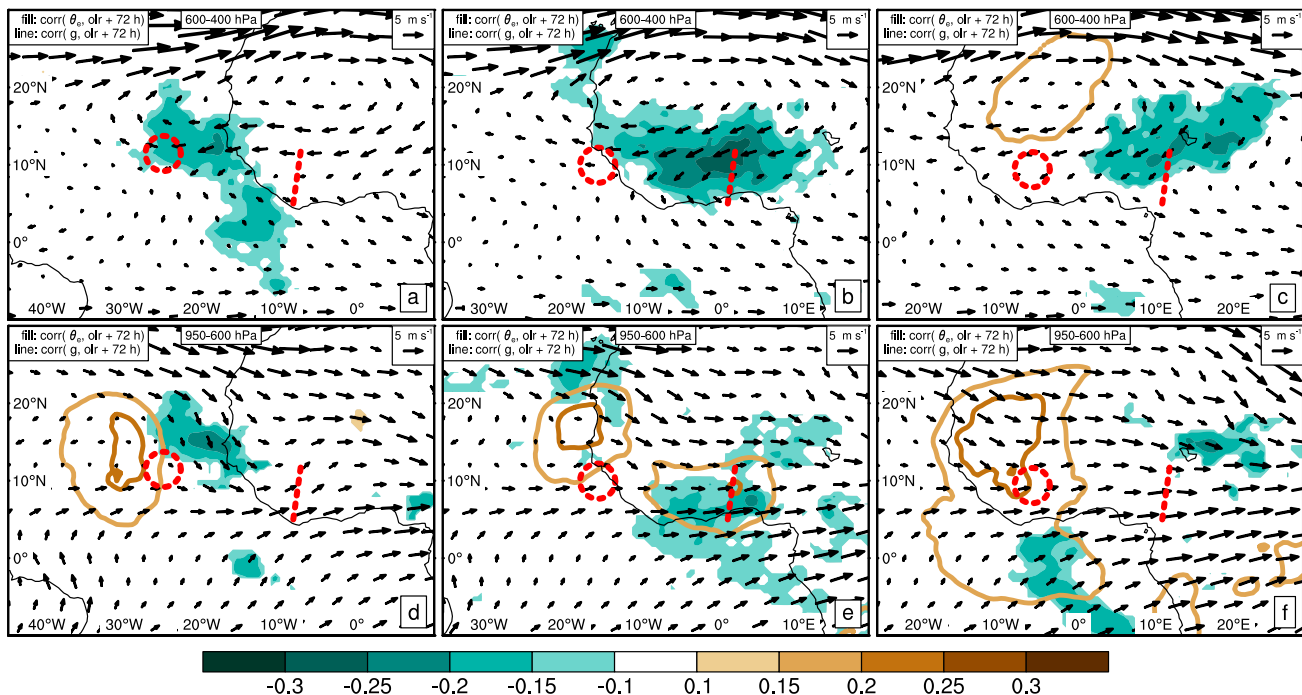


FIG. 9. Correlation of layer-averaged anomalous environmental variables at $t - 72$ h with anomalous daily OLR within 250 km of the trough centers. Plots show θ_e correlations (shaded), geopotential height correlation (contours), and wave-relative layer-averaged wind (vectors). (a)–(c) Midlevel (600–400 hPa) and (d)–(f) low-level (950–600 hPa) fields are shown. Columns show the three trough locations from west to east. The dashed red circle shows the region at hour 0 where the anomalous daily OLR was averaged within 250 km of the trough center. The dashed red line shows the approximate trough axis at $t - 72$ h. Only significant correlations are plotted (see text for details).

correlate variability in the environmental characteristics with OLR activity around the trough 3 days later.

d. AEW wave variability and environmental moisture differences

To assess whether the environmental characteristics around the trajectory source regions have significant impacts on the convection within the AEW troughs, a larger sample of objectively tracked waves ($n = 443$) were used to correlate anomalous OLR around the trough center with environmental characteristics 3 days earlier. Analysis here will use the same three locations as the previous sections to compare whether regional variations in the correlations match the results of the trajectory analysis. Across each location the distribution of anomalous OLR around the troughs is consistent with a median of around -10 K and an IQR of approximately 25 K (not shown).

Comparison of the composite structure of this larger subset of waves, reveals that qualitatively the two subsets are representative of each other (not shown). Both composites reveal a developing low-level vortex of the wave over the coastal region around the 700-hPa trough axis. The troughs in this composite are slightly weaker, due in part to the larger sample used and the selection

criteria for the subset of troughs used previously, which were defined based on intensity at the coastal location. The large-scale structure is comparable though and therefore source regions from the trajectory analysis should apply to these troughs as well.

Lagged correlation between the anomalous OLR activity around the AEW troughs and layer-averaged θ_e and geopotential height 3 days earlier is presented in Fig. 9. These figures only include areas of significant correlation. The p value for significance is determined using a false discovery rate of 0.1 for the area shown (Wilks 2006); the resulting p value varies per variable and per panel but ranges from 0.006 to 0.003 or 99.4% to 99.7%.

Over the eastern Atlantic (Figs. 9a,d) significant negative correlations west of the trough axis are observed indicating that the convection within the AEW trough is sensitive to changes in θ_e downstream of the trough. The sensitivity to θ_e at midlevels is generally spread from the southwest to the northwest (Fig. 9a) while at low levels the area of significant correlation is restricted to the northwest of the trough axis (Fig. 9d). Low-level geopotential height anomalies at this location show a positive correlation around 2000 km west of the trough axis. This distance is equal to the approximate

wavelength of an AEW and suggests that convectively active AEW troughs are influenced by the strength or existence of a downstream AEW trough. Positive correlation here indicates that a more intense downstream AEW trough (negative heights) is related to increased convection (negative OLR) in the subsequent trough. An AEW trough in this region would also suggest increased southerly flow, thus increasing the poleward advection of θ_e , suggesting that a downstream AEW may prime the environment for convection in the following trough.

For trough-based convection over the coastal region, significant correlation with θ_e 72 h earlier is concentrated around the area of the trough axis (near 0° ; Figs. 9d,e). At low levels, the area of weak but significant correlation with θ_e also extends to the south. Significant positive geopotential height anomalies are found downstream of the trough axis again indicating that the downstream trough is related to increased convection in the subsequent AEW trough. Low-level θ_e along the African coast, north of the convection, is also shown as a region of significant correlation at this time.

Farther east, for convection located near 6°W , the 72-h correlation shows that sensitivity to midlevel θ_e is located around the trough axis extending from the west to the north and northeast (Fig. 9c). At low levels, areas of weak but significant correlation are shown to the southwest of the trough axis and northeast (Fig. 9f). Once again the low-level signature of positive correlation between anomalous geopotential height and anomalous OLR activity 72 h later is evident approximately 2000 km west of the trough axis.

These correlation plots show that convective activity across 443 AEW troughs has significant sensitivity to the environmental characteristics over a time lag of at least 72 h. The maximum correlation values presented, although significant, are relatively low, showing that many factors influence the evolution of a synoptic-scale weather pattern. However, the regional pattern of correlation and the consistency between this correlation analysis and the trajectory analysis highlights one factor in how AEW troughs can be influenced by their surrounding environment. The areas highlighted in these plots line up with the shifting inflow patterns revealed by the trajectory analysis, showing that the sensitivity of the AEWs to the environment is location dependent. Over Africa the trajectories revealed predominantly midlevel inflow from the east and northeast with low-level inflow from the southwest. The correlation plots also highlight these areas. As the troughs leave West Africa, this sensitivity switches to the west and northwest of the trough, comparable to

the increasing inflow of trajectories shown from over the eastern Atlantic at low levels.

4. Discussion and conclusions

This study has shown the structure of AEW troughs through the use of kinematic trajectory analysis. Compositing trajectories over multiple events has highlighted consistent pathways for air approaching the AEW troughs and how these change as the AEWs propagate west. Through the use of cluster analysis, five distinct sources for environmental air were identified. Variability in the environmental characteristics of the trajectory source regions were then shown to be significantly correlated with convective activity around the AEW trough 3 days later. This analysis shows both a direct kinematic route for environmental characteristics that will be ingested and thus impact the AEW troughs, and the correlation of those characteristics with convective activity at later times.

The kinematic trajectory analysis highlighted that troughs over West Africa have different inflow routes between midlevels and low levels. Over West Africa midlevel (650–300 hPa) flow is primarily from around the trough (although over a large region of around 1000 km) or from the northeast associated with flow along the AEJ and northerly flow around the eastern edge of subtropical ridge over the Sahara. At low levels the main source of air is from the west and southwest associated with the background monsoonal flow over the region (Thorncroft et al. 2011; Lélé et al. 2015). As the troughs reach the West African coast, low-level inflow from the northwest also becomes a dominant route for environmental air to reach the trough center.

The trajectory analysis shows that flow from the northwest, over the eastern Atlantic, is characterized by low θ_e air, likely not of typical SAL origin and either from subtropical subsidence over the eastern Atlantic or midlatitude subsidence then advected south around the subtropical ridge. This low-level trade wind flow along the coast of West Africa becomes an increasingly important source region for trajectories as the AEW troughs cross the West African coastline. This source of low equivalent potential temperature air usually undercuts the warm and dry air associated with SAL outbreaks (Carlson and Prospero 1972). Because of the relatively shallow marine atmospheric boundary layer (MABL) over the eastern Atlantic, as low as 200 m (Lee et al. 2010; Fuhlbrügge et al. 2013), the northerly trade winds are therefore able to remain relatively dry and cool as they propagate south. This flow is therefore trapped between the strong vertical moisture gradient below at the top of the MABL and a strong temperature

inversion above, associated with the SAL. While the trajectory analysis in this research does not extend far enough back in time to determine whether this air is of tropical or midlatitude origin, trajectories in this region typically originate from either low-level air over Europe or subsiding air from North America and over the Atlantic (Lee et al. 2010; Fuhlbrügge et al. 2013). Schwendike et al. (2016) highlighted that variability in this low-level flow was an important factor in the evolution of Tropical Storm Helene (2006), while Brammer and Thorncroft (2015) showed that variability in the low-level moisture to the northwest of the AEW troughs was important for TC genesis over the eastern Atlantic. The analysis here in addition to the previous studies highlights the importance of dry air at low levels over the eastern Atlantic for the evolution of AEWs as they leave the West African coast. Dry air associated with SAL outbreaks has received a lot of attention in the literature; however, the trajectory analysis here shows that inflow, especially from the northwest, is more common at lower levels; below the typical base of the SAL structure. While there is inflow from the northeast, at midlevels, it takes a relatively long time to circulate around the trough.

The trajectory analysis here shows that air at midlevels, especially east of the trough, will take a longer route around the circulation and is less likely to be entrained. In developing cyclones, trajectories that take a cyclonic route around a strong vortex are either modified along their path or are not entrained due to the weak midlevel inflow, such that environmental dry air does not have a detrimental impact if or when reaching the vortex center (Braun et al. 2012; Fritz and Wang 2013). At levels where the circulation is weaker, however, dry air is able to penetrate the vortex center and can have negative impacts on the evolution of the system (e.g., Fritz and Wang 2013). As AEWs leave the West African coast the vorticity within the trough typically develops at lower levels (Janiga and Thorncroft 2013); therefore, the sensitivity of the troughs to the low-level environment may decrease as the troughs move over the main development region (Riemer and Montgomery 2011; Wang and Hanks 2014; Brammer and Thorncroft 2015).

The correlation analysis performed over a larger subset of waves confirms the impact of various source regions and levels determined by the trajectory analysis. Over West Africa the areas of greatest sensitivity for convection within the trough is at midlevels, near the trough axis, and to the northeast and southwest at low levels. These regions match the two main pathways of trajectories highlighted by the trajectory analysis. As the troughs propagate west, the sensitivity to the

environmental θ_e is observed shifting west of the trough axis and northwest at low levels, consistent with the regional changes of the inflow indicated by the trajectory analysis.

At each location positive correlation was also observed in geopotential height approximately 2000 km or an AEW wavelength downstream of the target AEW trough. This indicates that either the presence or intensity of a downstream AEW could influence convection in the following trough. Variability in the moisture field could likely be perturbed by the presence or intensity of a downstream wave increasing the southerly flux of high θ_e on its eastern edge. Over Africa, the variability in the midlevel θ_e field may be influenced by the strength and location of the Saharan heat low and/or midlatitude waves influencing the equatorward transport of dry air over the eastern Sahara (Chauvin et al. 2010).

The analysis does highlight that through kinematic trajectory analysis dominant trajectory pathways and source regions can be identified. Correlation analysis of environmental characteristics and convective activity within the AEW troughs has then independently linked these source regions with changes in convective activity at a lagged time.

The analysis here highlights the wave relative flow of AEW troughs as they transition from over West Africa to the Atlantic. This evolution shows the waves transitioning from a monsoonal flow regime with moist low-level inflow from the south and drier midlevel flow associated with the AEJ, to a more complex regime with low-level convergence of the moist flow from the south and dry low-level air from the north. It is suggested from the analysis here, and previous literature that considers the low-level trade wind flow over the eastern Atlantic, that the variability in this influx of cool and dry air from the northwest can be a crucial influence on AEWs as they leave West Africa. Further analysis utilizing high-resolution numerical experiments or ensemble-based guidance is needed to understand how this environmental influence impacts AEWs of varying strengths and the predictability of this evolution in numerical weather prediction models.

Acknowledgments. This research is supported by the NASA Grant NNX10AU44G on the Hurricane and Severe Storm Sentinel (HS3) field campaign. Analysis and plotting of data were conducted using the NCAR Command Language (version 6.3.0, 2015) (Brown et al. 2014). The CFSR data used in this study were downloaded from the Research Data Archive (RDA), which is maintained by the Computational and Information Systems Laboratory (CISL) at the National Center for

Atmospheric Research (Saha et al. 2014). NCAR is sponsored by the National Science Foundation (NSF). The original CFSR data are available from the RDA (<http://rda.ucar.edu>) in dataset numbers ds093.0. The authors also wish to thank the anonymous reviewers, whose thorough comments improved the research and clarity of this manuscript.

REFERENCES

- Berry, G. J., C. D. Thorncroft, and T. Hewson, 2007: African easterly waves during 2004—Analysis using objective techniques. *Mon. Wea. Rev.*, **135**, 1251–1267, doi:10.1175/MWR3343.1.
- Brammer, A., and C. D. Thorncroft, 2015: Variability and evolution of African easterly wave structures and their relationship with tropical cyclogenesis over the eastern Atlantic. *Mon. Wea. Rev.*, **143**, 4975–4995, doi:10.1175/MWR-D-15-0106.1.
- Braun, S. A., 2010: Reevaluating the role of the Saharan air layer in Atlantic tropical cyclogenesis and evolution. *Mon. Wea. Rev.*, **138**, 2007–2037, doi:10.1175/2009MWR3135.1.
- , J. A. Sippel, and D. S. Nolan, 2012: The impact of dry midlevel air on hurricane intensity in idealized simulations with no mean flow. *J. Atmos. Sci.*, **69**, 236–257, doi:10.1175/JAS-D-10-05007.1.
- Bretherton, C. S., M. E. Peters, and L. E. Back, 2004: Relationships between water vapor path and precipitation over the tropical oceans. *J. Climate*, **17**, 1517–1528, doi:10.1175/1520-0442(2004)017<1517:RBWVPA>2.0.CO;2.
- Brown, D., R. Brownrigg, M. Haley, and W. Huang, 2014: NCAR Command Language (version 6.3.0). UCAR/NCAR/CISL/TDD, Boulder, CO, accessed 20 March 2015, doi:10.5065/D6WD3XH5.
- Burpee, R., 1972: The origin and structure of easterly waves in the lower troposphere of North Africa. *J. Atmos. Sci.*, **29**, 77–90, doi:10.1175/1520-0469(1972)029<0077:TOASOE>2.0.CO;2.
- , 1974: Characteristics of North African easterly waves during the summers of 1968 and 1969. *J. Atmos. Sci.*, **31**, 1556–1570, doi:10.1175/1520-0469(1974)031<1556:CONAEW>2.0.CO;2.
- Cape, J. N., J. Methven, and L. E. Hudson, 2000: The use of trajectory cluster analysis to interpret trace gas measurements at Mace Head, Ireland. *Atmos. Environ.*, **34**, 3651–3663, doi:10.1016/S1352-2310(00)00098-4.
- Carlson, T. N., 1969: Synoptic histories of three African disturbances that developed into Atlantic hurricanes. *Mon. Wea. Rev.*, **97**, 256–276, doi:10.1175/1520-0493(1969)097<0256:SHOTAD>2.3.CO;2.
- , and J. M. Prospero, 1972: The large-scale movement of Saharan air outbreaks over the northern equatorial Atlantic. *J. Appl. Meteor.*, **11**, 283–297, doi:10.1175/1520-0450(1972)011<0283:TLSMOS>2.0.CO;2.
- Chauvin, F., R. Roehrig, and J.-P. Lafore, 2010: Intraseasonal variability of the Saharan heat low and its link with mid-latitudes. *J. Climate*, **23**, 2544–2561, doi:10.1175/2010JCLI3093.1.
- Dee, D. P., and Coauthors, 2011: The ERA-Interim reanalysis: Configuration and performance of the data assimilation system. *Quart. J. Roy. Meteor. Soc.*, **137**, 553–597, doi:10.1002/qj.828.
- Deshpande, R. D., M. Dave, V. Padhya, H. Kumar, and S. K. Gupta, 2015: Water vapour source identification for daily rain events at Ahmedabad in semi-arid western India: Wind trajectory analyses. *Meteor. Appl.*, **22**, 754–762, doi:10.1002/met.1515.
- Diedhiou, A., S. Janicot, A. Viltard, and P. De Felice, 2001: Composite patterns of easterly disturbances over West Africa and the tropical Atlantic: A climatology from the 1979–95 NCEP/NCAR reanalyses. *Climate Dyn.*, **18**, 241–253, doi:10.1007/s003820100173.
- Dorling, S. R., T. D. Davies, and C. E. Pierce, 1992: Cluster analysis: A technique for estimating the synoptic meteorological controls on air and precipitation chemistry—Method and applications. *Atmos. Environ.*, **26**, 2575–2581, doi:10.1016/0960-1686(92)90110-7.
- Draxler, R. R., and G. D. Hess, 1997: Description of the HYSPLIT_4 modeling system. NOAA Tech. Memo. ERL ARL-224, NOAA/Air Resources Laboratory, Silver Spring, MD, 27 pp. [Available online at <https://www.arl.noaa.gov/documents/reports/arl-224.pdf>.]
- , and —, 1998: An overview of the HYSPLIT_4 modeling system for trajectories, dispersion, and deposition. *Aust. Meteor. Mag.*, **47** (4), 295–308.
- Dunion, J. P., and C. S. Velden, 2004: The impact of the Saharan air layer on Atlantic tropical cyclone activity. *Bull. Amer. Meteor. Soc.*, **85**, 353–365, doi:10.1175/BAMS-85-3-353.
- Dunkerton, T., M. Montgomery, and Z. Wang, 2009: Tropical cyclogenesis in a tropical wave critical layer: Easterly waves. *Atmos. Chem. Phys.*, **9**, 5587–5646, doi:10.5194/acp-9-5587-2009.
- Duvel, J.-P., 1990: Convection over tropical Africa and the Atlantic Ocean during northern summer. Part II: Modulation by easterly waves. *Mon. Wea. Rev.*, **118**, 1855–1868, doi:10.1175/1520-0493(1990)118<1855:COTAAT>2.0.CO;2.
- Ersek, V., A. C. Mix, and P. U. Clark, 2010: Variations of $\delta^{18}\text{O}$ in rainwater from southwestern Oregon. *J. Geophys. Res.*, **115**, D09109, doi:10.1029/2009JD013345.
- Fink, A. H., and A. Reiner, 2003: Spatiotemporal variability of the relation between African easterly waves and West African squall lines in 1998 and 1999. *J. Geophys. Res.*, **108**, 4332, doi:10.1029/2002JD002816.
- , D. G. Vincent, P. M. Reiner, and P. Speth, 2004: Mean state and wave disturbances during phases I, II, and III of GATE based on ERA-40. *Mon. Wea. Rev.*, **132**, 1661–1683, doi:10.1175/1520-0493(2004)132<1661:MSAWDD>2.0.CO;2.
- Frank, N. L., 1969: The “inverted V” cloud pattern—An easterly wave? *Mon. Wea. Rev.*, **97**, 130–140, doi:10.1175/1520-0493(1969)097<0130:TVCPEW>2.3.CO;2.
- Fritz, C., and Z. Wang, 2013: A numerical study of the impacts of dry air on tropical cyclone formation: A development case and a nondevelopment case. *J. Atmos. Sci.*, **70**, 91–111, doi:10.1175/JAS-D-12-018.1.
- Fuhlbrügge, S., K. Krüger, B. Quack, E. Atlas, H. Hepach, and F. Ziska, 2013: Impact of the marine atmospheric boundary layer conditions on VSLS abundances in the eastern tropical and subtropical North Atlantic Ocean. *Atmos. Chem. Phys.*, **13**, 6345–6357, doi:10.5194/acp-13-6345-2013.
- Galarneau, T. J., Jr., L. F. Bosart, and R. S. Schumacher, 2010: Predecessor rain events ahead of tropical cyclones. *Mon. Wea. Rev.*, **138**, 3272–3297, doi:10.1175/2010MWR3243.1.
- Gu, G., R. F. Adler, G. J. Huffman, and S. Curtis, 2004: African easterly waves and their association with precipitation. *J. Geophys. Res.*, **109**, D04101, doi:10.1029/2003JD003967.
- Harris, J. M., and J. D. Kahl, 1990: A descriptive atmospheric transport climatology for the Mauna Loa Observatory, using

- clustered trajectories. *J. Geophys. Res.*, **95**, 13 651–13 667, doi:10.1029/JD095iD09p13651.
- , R. R. Draxler, and S. J. Oltmans, 2005: Trajectory model sensitivity to differences in input data and vertical transport method. *J. Geophys. Res.*, **110**, D14109, doi:10.1029/2004JD005750.
- Huffman, G. J., and Coauthors, 2007: The TRMM Multisatellite Precipitation Analysis (TMPA): Quasi-global, multiyear, combined-sensor precipitation estimates at fine scales. *J. Hydrometeorol.*, **8**, 38–55, doi:10.1175/JHM560.1.
- Janiga, M. A., and C. D. Thorncroft, 2013: Regional differences in the kinematic and thermodynamic structure of African easterly waves. *Quart. J. Roy. Meteor. Soc.*, **139**, 1598–1614, doi:10.1002/qj.2047.
- , and —, 2016: The influence of African easterly waves on convection over tropical Africa and the east Atlantic. *Mon. Wea. Rev.*, **144**, 171–192, doi:10.1175/MWR-D-14-00419.1.
- Karyampudi, V. M., and T. N. Carlson, 1988: Analysis and numerical simulations of the Saharan air layer and its effect on easterly wave disturbances. *J. Atmos. Sci.*, **45**, 3102–3136, doi:10.1175/1520-0469(1988)045<3102:AANSOT>2.0.CO;2.
- Kassomenos, P., S. Vardoulakis, R. Borge, J. Lumbreras, C. Papaloukas, and S. Karakitsios, 2010: Comparison of statistical clustering techniques for the classification of modelled atmospheric trajectories. *Theor. Appl. Climatol.*, **102**, 1–12, doi:10.1007/s00704-009-0233-7.
- Kiladis, G. N., C. D. Thorncroft, and N. M. J. Hall, 2006: Three-dimensional structure and dynamics of African easterly waves. Part I: Observations. *J. Atmos. Sci.*, **63**, 2212–2230, doi:10.1175/JAS3741.1.
- Lee, H.-T., 2011: NOAA climate data record (CDR) of daily outgoing longwave radiation (OLR). NOAA/National Climatic Data Center, NOAA CDR Program, accessed 1 July 2016, doi:10.7289/V5SJ1HH2.
- , C. J. Schreck III, and K. R. Knapp, 2014: Generation of the daily OLR climate data record. *Proc. EUMETSAT Meteorological Satellite Conf.*, Geneva, Switzerland, EUMETSAT. [Available online at http://olr.umd.edu/References/Lee_2014_Generation_of_Daily_OLR_CDR_Eumetsat_Sep2014.pdf.]
- Lee, J. D., and Coauthors, 2010: Reactive Halogens in the Marine Boundary Layer (RHAMBLe): The tropical North Atlantic experiments. *Atmos. Chem. Phys.*, **10**, 1031–1055, doi:10.5194/acp-10-1031-2010.
- Lélé, M. I., L. M. Leslie, and P. J. Lamb, 2015: Analysis of low-level atmospheric moisture transport associated with the West African monsoon. *J. Climate*, **28**, 4414–4430, doi:10.1175/JCLI-D-14-00746.1.
- MacQueen, J., 1967: Some methods for classification and analysis of multivariate observations. *Statistics*, L. M. Le Cam and J. Neyman, Eds., Vol. 1, *Proceedings of the Fifth Berkeley Symposium on Mathematical Statistics and Probability*, University of California Press, 281–297.
- Merrill, J. T., R. Bleck, and L. Avila, 1985: Modeling atmospheric transport to the Marshall Islands. *J. Geophys. Res.*, **90**, 12 927–12 936, doi:10.1029/JD090iD07p12927.
- Moody, J. L., and J. N. Galloway, 1988: Quantifying the relationship between atmospheric transport and the chemical composition of precipitation on Bermuda. *Tellus*, **40B**, 463–479, doi:10.3402/tellusb.v40i5.16014.
- Payne, S. W., and M. M. McGarry, 1977: The relationship of satellite inferred convective activity to easterly waves over West Africa and the adjacent ocean during phase III of GATE. *Mon. Wea. Rev.*, **105**, 413–420, doi:10.1175/1520-0493(1977)105<0413:TROSIC>2.0.CO;2.
- Pierrehumbert, R. T., and R. Roca, 1998: Evidence for control of Atlantic subtropical humidity by large scale advection. *Geophys. Res. Lett.*, **25**, 4537–4540, doi:10.1029/1998GL900203.
- Poan, D. E., R. Roehrig, F. Couvreur, and J.-P. Lafore, 2013: West African monsoon intraseasonal variability: A precipitable water perspective. *J. Atmos. Sci.*, **70**, 1035–1052, doi:10.1175/JAS-D-12-087.1.
- Prospero, J. M., and T. N. Carlson, 1972: Vertical and areal distribution of Saharan dust over the western equatorial North Atlantic Ocean. *J. Geophys. Res.*, **77**, 5255–5265, doi:10.1029/JC077i027p05255.
- Reale, O., K. M. Lau, A. Silva, and T. Matsui, 2014: Impact of assimilated and interactive aerosol on tropical cyclogenesis. *Geophys. Res. Lett.*, **41**, 3282–3288, doi:10.1002/2014GL059918.
- Reed, R. J., D. C. Norquist, and E. E. Recker, 1977: The structure and properties of African wave disturbances as observed during phase III of GATE. *Mon. Wea. Rev.*, **105**, 317–333, doi:10.1175/1520-0493(1977)105<0317:TSAPOA>2.0.CO;2.
- Riemer, M., and M. T. Montgomery, 2011: Simple kinematic models for the environmental interaction of tropical cyclones in vertical wind shear. *Atmos. Chem. Phys.*, **11**, 9395–9414, doi:10.5194/acp-11-9395-2011.
- Rios-Berrios, R., R. D. Torn, and C. A. Davis, 2016: An ensemble approach to investigate tropical cyclone intensification in sheared environments. Part I: Katia (2011). *J. Atmos. Sci.*, **73**, 71–93, doi:10.1175/JAS-D-15-0052.1.
- Roberts, A. J., J. H. Marsham, and P. Knippertz, 2015: Disagreements in low-level moisture between (re)analyses over summertime West Africa. *Mon. Wea. Rev.*, **143**, 1193–1211, doi:10.1175/MWR-D-14-00218.1.
- Roca, R., J. P. Lafore, C. Piriou, and J.-L. Redelsperger, 2005: Extratropical dry-air intrusions into the West African monsoon midtroposphere: An important factor for the convective activity over the Sahel. *J. Atmos. Sci.*, **62**, 390–407, doi:10.1175/JAS-3366.1.
- Saha, S., and Coauthors, 2010: The NCEP Climate Forecast System Reanalysis. *Bull. Amer. Meteor. Soc.*, **91**, 1015–1057, doi:10.1175/2010BAMS3001.1.
- , and Coauthors, 2014: The NCEP Climate Forecast System version 2. *J. Climate*, **27**, 2185–2208, doi:10.1175/JCLI-D-12-00823.1.
- Schenkel, B. A., and R. E. Hart, 2015: An analysis of the environmental moisture impacts of western North Pacific tropical cyclones. *J. Climate*, **28**, 2600–2622, doi:10.1175/JCLI-D-14-00213.1.
- Schwendike, J., S. C. Jones, B. Vogel, and H. Vogel, 2016: Mineral dust transport toward Hurricane Helene (2006). *J. Geophys. Res. Atmos.*, **121**, 5538–5566, doi:10.1002/2015JD024708.
- Sjostrom, D. J., and J. M. Welker, 2009: The influence of air mass source on the seasonal isotopic composition of precipitation, eastern USA. *J. Geochem. Explor.*, **102**, 103–112, doi:10.1016/j.gexplo.2009.03.001.
- Stein, A. F., R. R. Draxler, G. D. Rolph, B. B. Stunder, M. D. Cohen, and F. F. Ngan, 2015: NOAA's HYSPLIT Atmospheric Transport and Dispersion Modeling System. *Bull. Amer. Meteor. Soc.*, **96**, 2059–2077, doi:10.1175/BAMS-D-14-00110.1.
- Stohl, A., and P. Seibert, 1998: Accuracy of trajectories as determined from the conservation of meteorological tracers. *Quart. J. Roy. Meteor. Soc.*, **124**, 1465–1484, doi:10.1002/qj.49712454907.

- , G. Wotawa, P. Seibert, and H. Kromp-Kolb, 1995: Interpolation errors in wind fields as a function of spatial and temporal resolution and their impact on different types of kinematic trajectories. *J. Appl. Meteor.*, **34**, 2149–2165, doi:10.1175/1520-0450(1995)034<2149:IEIWFA>2.0.CO;2.
- Thompson, R. M., S. W. Payne, E. E. Recker, and R. J. Reed, 1979: Structure and properties of synoptic-scale wave disturbances in the intertropical convergence zone of the eastern Atlantic. *J. Atmos. Sci.*, **36**, 53–72, doi:10.1175/1520-0469(1979)036<0053:SAPOSS>2.0.CO;2.
- Thorncroft, C. D., and B. J. Hoskins, 1994: An idealized study of African easterly waves. I: A linear view. *Quart. J. Roy. Meteor. Soc.*, **120**, 953–982, doi:10.1002/qj.49712051809.
- , H. Nguyen, C. Zhang, and P. Peyrillé, 2011: Annual cycle of the West African monsoon: Regional circulations and associated water vapour transport. *Quart. J. Roy. Meteor. Soc.*, **137**, 129–147, doi:10.1002/qj.728.
- Wang, Z., and I. Hanks, 2014: Characteristics of tropical easterly wave pouches during tropical cyclone formation. *Mon. Wea. Rev.*, **142**, 626–633, doi:10.1175/MWR-D-13-00267.1.
- , M. T. Montgomery, and T. Dunkerton, 2010: Genesis of Pre-Hurricane Felix (2007). Part I: The role of the easterly wave critical layer. *J. Atmos. Sci.*, **67**, 1711–1729, doi:10.1175/2009JAS3420.1.
- Wilks, D. S., 2006: On “field significance” and the false discovery rate. *J. Appl. Meteor. Climatol.*, **45**, 1181–1189, doi:10.1175/JAM2404.1.
- Witten, D. M., and R. Tibshirani, 2010: A framework for feature selection in clustering. *J. Amer. Stat. Assoc.*, **105**, 713–726, doi:10.1198/jasa.2010.tm09415.